Stochastic Modeling of an Infectious Disease
Part II: Simulation Experiments and Verification of the Analysis.

Hisashi Kobayashi*
Dept. of Electrical Engineering
Princeton University
Princeton, NJ 08544, U.S.A.

August 5, 2020

Abstract

In [1], we introduced a *stochastic model* of an infectious disease, based on the *birth-and-death-with-immigration* (BDI) process. The model can capture the essence of dynamics of an infection process. The most significant finding is that the *time-dependent* (or transient) probability distribution of the infected population size is *negative binomial distributed* at all times with a very long tail distribution. Consequently, an epidemic pattern exhibits a much larger variation than has been assumed by most modeling experts, including the epidemiology community.

In this report, Part II, simulation runs and their interpretations are presented to support the above finding. The sample paths of different simulation runs exhibit indeed enormous variations, which confirms our analysis.

The epidemic pattern that a given environment (e.g., city or country) experiences is merely one *sample path* out of infinitely many possible paths. The enormous variations we observe in these simulation runs explain why some cities and countries experience much fewer infections and casualties than others. The size of the infected or dead populations could differ by factor of 100 or more even under identical conditions.

There are two important implications of our findings. First, it would be a futile effort to attempt to identify all possible causes or reasons why environments of similar situations differ so much in terms of epidemic patterns and the number of casualties. Our stochastic model suggests that "luck" or "chances" play a more significant role than most of us would be led to believe. Second, we should be prepared for a worst possible scenarios, which a stochastic model can provide with some probabilistic qualification (rather a single prediction curve), such as a 95 percent confidence range.

For all these probabilistic arguments, however, our stochastic model also shows that the infection process will immediately start declining, with no enertia whatsoever, once the exponential parameter $a = \lambda - \mu$ should turn negative. This result will be discussed in full, by both analysis and simulation in Part III, where we assume the infection rate parameter λ and the recovery (which includes removal and death) parameter μ are arbitrary functions of time.

*The Sherman Fairchild University Professor of Electrical Engineering and Computer Science, Emeritus, Email: Hisashi@Princeton.EDU, Home page: `https.hp.HisashiKobayashi.com`

Keywords: Birth-and-death process with immigration (BDI), Event-driven simulation, Sample paths of the processes $I(t)$, $R(t)$ and $R(t)$, New infections for each day, The death process $D(t)$. Percentile curves, non-zero initial condition.

Contents

1 Recapitulation of Part I

Our model formulation began with the set of linear differential-difference equations (Part I, page 8, replicated below in (4) and (5)) for the probability mass function (PMF)

$$P_n(t) \triangleq \Pr[I(t) = n], \quad n = 0, 1, 2, \cdots, \quad t \geq 0, \tag{1}$$

where $I(t)$ is the number of *infected, hence infectious persons*, at time t. We can express $I(t)$ as

$$I(t) = I_0 + A(t) + B(t) - R(t), \tag{2}$$

where I_0 is the initial value:

$$I(0) = I_0, \tag{3}$$

and

1. $A(t)$ is the *cumulative count* of infected arrivals from the outside. We assume the arrival pattern is completely random, i.e., a Poisson process with rate ν [persons/day].

2. $B(t)$ is the *cumulative count* of the infections that occur in the interval $[0, t]$. An infection occurs at the rate λ [person/day/infectious person].

3. $R(t)$ is the *cumulative count* of the infected persons who recover, are removed or die in $[0, t]$. This event occurs at the rate μ [persons/day/infected person].

The $P_n(t), n = 0, 1, 2, \cdots$ should satisfy the following set of differential equations:

$$\frac{dP_0(t)}{dt} = -\nu P_0(t) + \mu P_1(t), \tag{4}$$

$$\frac{dP_n(t)}{dt} = [(n-1)\lambda + \nu]P_{n-1}(t) - [n(\lambda+\mu)+\nu]P_n(t) + (n+1)\mu P_{n+1}(t), \quad n = 1, 2, 3. \cdots, \tag{5}$$

with the initial condition (3).

In order to find solve the above differential equations, we use the *probability generating function* (PGF) defined by

$$G(z, t) \triangleq \mathsf{E}[z^{I(t)}] = \sum_{n=0}^{\infty} P_n(t) z^n, \tag{6}$$

The set of differential equations (4) and (5) are then transformed into one *partial differential equation* (PDE):

$$\frac{\partial G(z,t)}{\partial t} = (z-1)\left[(\lambda z - \mu)\frac{\partial G(z,t)}{\partial z} + \nu G(z,t)\right], \tag{7}$$

with the condition

$$G(z, 0) = z^{I_0}. \tag{8}$$

We apply Lagrange's method to the above PDE, obtaining

$$G(z,t) = \left(\frac{a}{\lambda z - \mu - \lambda(z-1)e^{at}}\right)^r \left(\frac{\lambda z - \mu - \mu(z-1)e^{at}}{\lambda z - \mu - \lambda(z-1)e^{at}}\right)^{I_0}, \tag{9}$$

where

$$a \triangleq \lambda - \mu, \quad \text{and} \quad r \triangleq \frac{\nu}{\lambda}. \tag{10}$$

If $I_0 = 0$, (9) reduces to

$$G(z,t) = \left(\frac{a}{\lambda z - \mu - \lambda(z-1)e^{at}}\right)^r = \left(\frac{1-\beta(t)}{1-\beta(t)z}\right)^r, \tag{11}$$

where

$$\beta(t) \triangleq \frac{\lambda(e^{at}-1)}{\lambda e^{at} - \mu}. \tag{12}$$

To obtain $\mathsf{E}[I(t)] = \overline{I}(t)$, we use the formula $\mathsf{E}[I(t)] = \left.\frac{\partial G(z,t)}{\partial z}\right|_{z=1}$:

$$\overline{I}(t) = \frac{r\beta(t)}{1-\beta(t)} = \frac{\nu}{a}(e^{at}-1), \quad \text{where.} \tag{13}$$

It would be easy to observe that

- If $a > 0$, $\overline{I}(t)$ grows exponentially to infinity, as $t \to \infty$;
- If $a < 0$, it converges to $-\frac{\nu}{a} > 0$.
- If $a = 0$, $\overline{I}(t) = \nu t$ for all $t \geq 0$.

Let T [days] be the number of days that is required for $\overline{I}(t)$ to double. Then from (13), we find

$$e^{aT} = 2, \quad \text{or} \quad aT = \ln 2 = 0.693. \tag{14}$$

If $a = 0.2$ [day^{-1}] (as in the running example of Part I and the present paper), $\overline{I}(t)$ doubles in every $T \approx 3.5$ [days], hence quadruples every week.[1]

In order to generate the PMFs $P_n(t)$, by referring to the definition of the PGF (6), we differentiate $G(z,t)$ (11) w.r.t. z, set $z = 0$, divide the resulting expression by $n!$. That is

$$\begin{aligned}
P_0(t) &= G(0,t) = (1-\beta(t))^r \\
P_1(t) &= \left.\frac{\partial G(z,t)}{\partial z}\right|_{z=0} = (1-\beta(t))^r r\beta(t) \\
P_2(t) &= \left.\frac{1}{2!}\frac{\partial^2 G(z,t)}{\partial z^2}\right|_{z=0} = (1-\beta(t))^r \frac{(r+1)r}{2!}\beta(t)^2 \\
&\vdots \\
P_n(t) &= \left.\frac{1}{n!}\frac{\partial^n G(z,t)}{\partial z^n}\right|_{z=0} = (1-\beta(t))^r \frac{(n+r-1)\cdots(r+1)r}{n!}\beta(t)^n,
\end{aligned} \tag{15}$$

which we can write as

$$\boxed{P_n(t) = K(n,r)(1-\beta(t))^r \beta(t)^n, \quad n = 0,1,2,\cdots,} \tag{16}$$

where $K(n,r)$ is the binomial coefficient:

$$K(n,r) = \frac{(n+r-1)(n+r-2)\cdots(r+1)r}{n!} \triangleq \binom{n+r-1}{n}. \tag{17}$$

The above distribution $P_n(t)$ takes the form of a *Pascal distribution*, or *negative binomial distribution* (NBD), often denoted as NB(k,q), which is the probability of the number of failures n in Bernoulli trials needed to achieve k successes, where q is the probability of failure per trial

$$P_n^{NBD} = K(n,k)(1-q)^k q^n, \quad n = 0,1,2,\cdots. \tag{18}$$

The PGF of this NBD is given by

$$G_{NBD}(z) \triangleq \sum_{n=0}^{\infty} P_n^{NBD} z^n = \left(\frac{1-q}{1-qz}\right)^k. \tag{19}$$

[1] When the exponential growth rate in the environment of your interest differs from our example, you can still interpret our simulation results meaningfully. For example if $\overline{I}(t)$ double every week in the environment of your interest, you can scale the time axis by factor of two, i.e., $t = 0,1,2\cdots,50$ in our simulation plots, you assign different time scale, $t' = 0,2,4,\cdots,25$.

Thus, by equating $k = r \triangleq \frac{\nu}{\lambda}$ and $q = \beta(t)$, we see from (11) that the BDI process $I(t)$ is negative binomial distributed according to NB$(r, \beta(t))$ at given t.

We note the following properties of $K(n, r)$ (17) and the NBD (16):

i $K(0, r) = 1$, thus $P_0(t) = (1 - \beta(t))^r$ for all $t \geq 0$.

ii $K(1, r) = r$, thus $P_1(t) = r(1 - \beta(t))^r \beta(t)$. Therefore, $P_1(t) = r\beta(t)P_0(t)$.

iii $K(n, 1) = 1$ for all n. Then the PMF reduces to a geometric distribution $(1 - q)q^n$ with $q = \beta(t)$

iv $K(n, 2) = n + 1$ for all n;

v If $r < 1$, then $K(n, r) < 1$ for all $n \geq 0$. From Property ii and (16), we find that for each t, the PMF $P_n(t)$ is a monotone decreasing function of n, i.e., $P_n(t) \propto \beta(t)^n$, where $\beta(t)$ approaches 1 from below as t becomes large.

vi If $1 < r < 2$, then $K(n, r)$ is a monotone increasing concave (i.e., convex cap) function of n, bounded by $1 < K(n, r) < n + 1$.

vii If $r > 2$, then $K(n, r)$ is a monotone increasing convex function of n, bounded from below $K(n, r) > n + 1$.

viii By using Stirling's approximation for factorials and the Gamma function,

$$\Gamma(n + 1) = n! \approx \sqrt{2\pi n} \left(\frac{n}{e}\right)^n, \quad \text{for} \quad n > 1, \tag{20}$$

we can approximate $K(n, r)$, for $n > 1$ and $r > 1$, by

$$K(n, r) \approx \sqrt{\frac{1}{2\pi}} \frac{(n + r - 1)^{n+r-1}}{(r - 1)^{r-1} n^n}. \tag{21}$$

Thus, if r is small, e.g., $r \approx 1$, the distribution of (16), for any given t, slowly decreases towards zero as n increases. Thus, the distribution has a *long tail*) (see Figures 7-12 of Part I). Consequently, different *sample paths* of $I(t)$ are expected to exhibit enormous disparities, as will be shown in the next section, where we present simulation results, which demonstrate huge spreads across different sample paths.

It goes without saying that the most decisive factor that shapes the epidemic pattern is the exponential parameter $a = \lambda - \mu$. However, for a given a, different simulation runs show enormous differences in their infectious patterns. This wild random behavior is perhaps well beyond what even most epidemiologists are cognizant of. In other words, we should accept that we won't be able to find out all factors that can explain why some cities or countries are experiencing more hardship than others in terms of the number of infections and death tolls.

This also implies that Japan and other countries that have have observed a relatively small number of infections and casualties should be aware that they may not be as fortunate in new waves of the pandemic. They should be well prepared for the worst case scenario in order to protect their citizens.

In order to be able to provide specifically what will be the worst possible scenario, we need to come up with an accurate estimates of the model parameters λ, ν and ν, by carefully analyzing real and reliable data, and make the most likely estimates (or ranges of estimate), which will be the main focus in Part V [2] of our report.

2 Simulation of the proposed Stochastic Model

Simulations are often used when analytic techniques to estimate or predict the performance of a complex system are hard to come by. So-called *Monte-Carlo simulation* techniques, such as *variance reduction techniques*, are often adopted to estimate a given performance measure accurately and efficiently. The main purpose of our simulation experiments here, however, is different from these situations in that we fortunately have obtained an exact analytic result of the system, i.e., we have found closed-form expressions for the PMFs $P_n(t)$'s by solving a partial differential equation.

We present here the results of various simulation runs primarily to better explain and demonstrate the validity and utility of our stochastic model. Plots of various sample paths of our simulation experiments should serve as a convincing and understandable evidence to support our model.

2.1 Description of the simulation model

We shall briefly describe how our simulator is designed for the benefit of some readers who may not be sufficiently familiar with probabilistic simulation [2] of a Markov process such as the birth-death-immigration process. We adopt the *time-asynchronous* approach as opposed to the time-synchronous approach, which may be more suited to simulating events that occur periodically at predetermined moments, such as seen in time-synchronous communication systems. The time-asynchronous approach is also referred to as the *event-scheduling* approach.

In our model, there are three types of events; (A) an arrival of an infected person from the outside; (B) an infection caused by an infectious person; and (R) a recovery/removal/death of an infected person.

The random process $I(t)$ defined by the differential equations (4) and (5) is a Markov process. At an arbitrarily given time t, when $I(t) = n$, the time interval until the next event is a random variable (RV) X with a negative exponential distribution of mean $1/\gamma(n)$, [3] where

$$\gamma(n) = n(\lambda + \mu) + \nu. \tag{22}$$

That is, the distribution function of the RV X is

$$F_X(x) \triangleq \Pr[X \le x] = 1 - e^{-\gamma(n)x}. \tag{23}$$

Generation of instances of the random variable X can be done by calling the *random number generator* (RNG) that is available in almost all programming languages, including MATLAB.[4] It will generate an instances u of the random variable U, which is uniformly distributed between 0 and 1. Then we transform u by the function $F_X^{-1}(\cdot)$, i.e., find x such that $u = F_X(x) = 1 - e^{-\gamma(n)x}$. In other words, $x = \log(1-u)/\gamma(n)$. Since u is uniformly distributed between 0 and 1, so is $1-u$, thus $x' \triangleq \log u/\gamma(n)$ can be used instead of x,

[2] As for detailed discussion of simulation techniques, see e.g., [3], Chapter 4, [4], Chapter 16.

[3] Note that $[n(\lambda+\mu)+\nu]$ is the coefficient of the $P_n(t)$ term in the RHS of differential equation of $P_n(t)$ (5).

[4] The random number generator used today in MATLAB, Python, Pokemon, and others is what is known as Mersenne Twisted GFSR(general feedback shift register) sequence, developed by Makoto Matsumoto and Takuji Nishimoto ("Mersenne Twister: a 623-dimensionally equidistributed uniform pseudo-random number generator," *ACM Transactions on Modelling and Computer Simulation*, January 1998). This algorithm generates a pseudo-random sequence of the period $2^{19937} - 1$, and the implementation is abbreviated as MT19937. It uses a Mersenne prime number M, of the form $M = 2^n - 1$, for some integer n. Sometimes n is restricted to a prime number, as well.

At the occurrence of an event, we classify it as one of the three types of events as follows: choose type-(A) with probability $P_A \triangleq \nu/\gamma(n)$; choose type-(B) with probability $P_B = n\lambda/\gamma(n)$; and choose type-(R) with probability $P_R = 1 - P_A - P_B = n\mu/\gamma(n)$. Note that if $n = 0$, then $P_A = 1$, and $P_B = P_R - 0$.

The rationale for this extremely simple event scheduling approach is that the Poisson process possesses the following beautiful properties: (a) the *memoryless property*, (b) the *reproductive additivity*, and (c) the *decomposition* property.[5]

Thus, the core of our simulation program is as follows.

1. If $I(t) = 0$, then $\gamma(0) = \nu$, hence, the only possible event to consider is a type-(A) event. The time until the next arrival, x, is determined by $x = \log u/\nu$, where $u \in [0, 1]$ is an output drawn from the RNG. Advance the clock time to $t' \triangleq t + x$, and increment $A(t)$ by 1 for $t \geq t'$.

2. If $I(t) = n \geq 1$, the next event can be any of the three types. The time-interval until the next event is determined by $x = \log u/gamma(n)$T, where $u \in [0, 1]$ as defined above. Take another RNG output $u' \in [0, 1]$. Classify the event as type-(A), if $0 \leq u' \leq P_A$: classify it as a type-(B) event, if $P_A < u' \leq P_A + P_B$; and classify it as type-(R), if $P_A + P_B < u' \leq 1$ Advance the simulation clock to $t' \triangleq t + x$, and increment the counter $A(t), B(t)$ or $R(t)$ by one depending on the classified result is type (A), (B) or (R).

3. Go back to step 1 or 2, depending $I(t') = 0$ or $I(t') \geq 1$, and use t' as a new clock time, and repeat the above steps.

2.2 Percentiles plots for the expected spread of simulation curves

As we discussed in Part I, the ratio of the standard deviation of a given probability distribution to its mean, called the *coefficient of variation* (CV), sometimes serve as a simple and good measure of the dispersion of the distribution. We obtained the CV of the distribution of $I(t)$ in the BDI model, as given in (74) in Part I.

If the distribution of a random variable X is close to a normal (or Gaussian) distribution, it is well known that realizations of X fall within the mean $\pm\sigma_X$ with the probability .68. Similarly, the mean $\pm 2\sigma_X$ provides a 98% confidence interval. But this rule of thumb does not apply to the NB(r, q) with small r, because the distribution is highly skewed, far from being symmetrical around the mean. A more accurate and reliable way is to compare simulation plots with the percentile curves of the NB(r, q). To that end, we need to calculate the *cumulative distribution function* (CDF) by

$$F_{BDI}(x, t) \triangleq \Pr[N(t) \leq x] = \sum_{n=0}^{\lfloor x \rfloor} P_n(t), \tag{24}$$

[5]The property (a) has to do with the memoryless property of the variable X which has an exponential distribution. Assume that Y time units have elapsed since the last arrival. The time until the next arrival $R \triangleq X - Y$ has the same exponential distribution as X, regardless of Y. The property (b) means that when m independent Poisson processes with rate $\lambda_k, k = 1, 2, \cdots, m$ are merged, the resulting stream is another Poisson process with rate $\sum_{k=1}^{m} \lambda_k$. The property (c) is an opposite of the property (b). If a Poisson process with rate λ is split into m sub-streams, by assigning each arrival independently into the kth sub-stream with probability p_k, where $\sum_{k=1}^{m} p_k = 1$. Then the sub-streams are independent Poisson processes with rate $p_k\lambda$'s. For proofs of these properties, see e.g. [5], pp. 403-405).

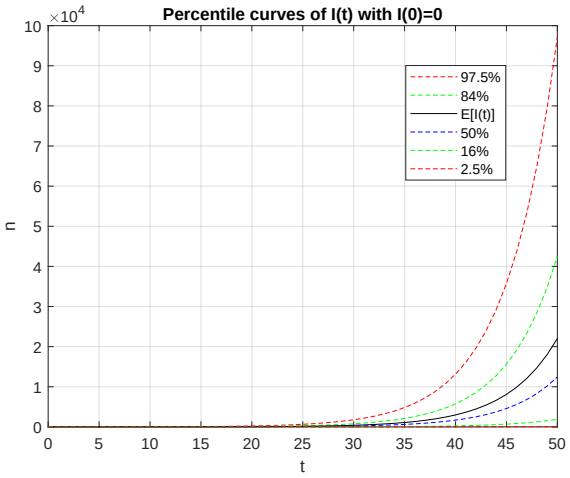

Figure 1: Percentile curves of $P_n(t)$ of $I(t)$for $0 \le t \le 50$, $\lambda = 0.3, \mu = 0.1, \nu = 0.2$.

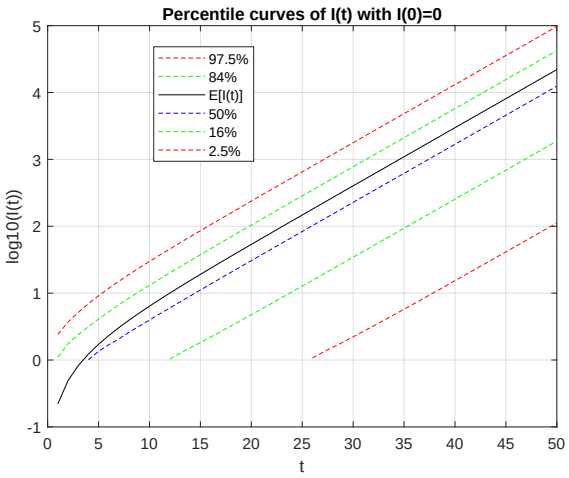

Figure 2: Semi-log plot of the percentile curves for $0 \le t \le 50$, $\lambda = 0.3, \mu = 0.1, \nu = 0.2$.

where $P_n(t)$ is the PMF of (16) and $\lfloor x \rfloor$ is the largest integer, not exceeding x. Figure 1 shows the curves where the CDF take 0.975, and 0.025 (in red dash curves), 0.84 and 0.16 (in green dash) and 0.5 (in blue dash). The stochastic mean $E[I(t)] \triangleq \overline{I}(t)$ is shown in black solid curve.

We can expect that if we conduct many simulation experiments, about 68% of the sample paths will fall within the region between the green dashed curves, and about 95% of the sample paths should fall within the range given by the two red dashed curves. Roughly one half of the simulation curves should be above the blue dashed curve and the other half should be below this curve. Note that the stochastic mean curve is appreciably above the median (50%) curve: nearly by a factor of two.

Note that the top curve (the upper half of the 95% confidence interval) climbs up to as large as 100,000 by the 50th day, while it is only 1,800 on the 30th day. This is the power of the exponential growth, with which we are all familiar now by observing how rapidly the Covid-19's infections have grown in many part of the world.

2.3 Simulation results

2.3.1 Simulation of the process $I(t)$, the number of infections at time t

We present the results of six simulation runs in Figure 3, where we superimpose the percentile curves presented in the previous section. Five out of the six runs are within the 68% confidence interval, (between the two green dashed curves), but Run 4 exceeds the 97.5 percentile curve by a rather big margin. In order to show the behavior more clearly in the initial rising phase of the process $I(t)$ (i.e., for small t) we present the semi-log plots of the same six runs in Figures 6. We conducted many more simulation runs, but will not include them in this report for the interest of space.

2.3.2 Simulation of the external arrivals $A(t)$

Figure 8 show arrival patterns. The Poisson distribution of mean λ has the variance equal to the mean: $\sigma^2 = \lambda$; and for large λ, its CDF (cumulative distribution function) converges to that of the

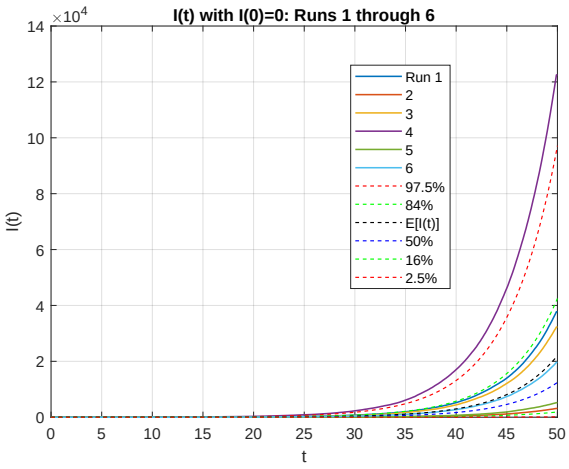

Figure 3: Simulated $I(t)$ process, Runs 1-6; $\lambda = 0.3, \mu = 0.1, \nu = 0.2$.

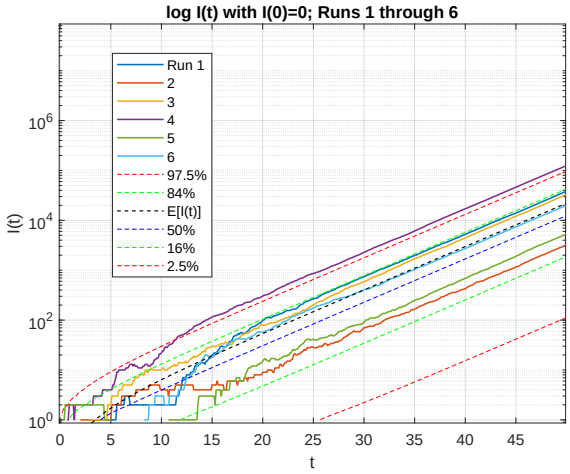

Figure 4: Semi-log plots of simulated $I(t)$ process, Runs 1-6; $\lambda = 0.3, \mu = 0.1, \nu = 0.2$.

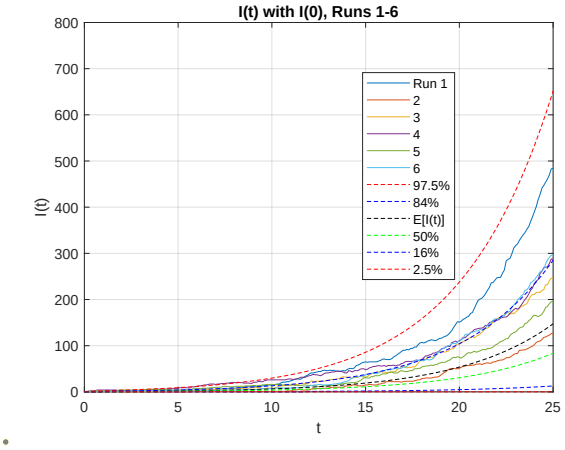

Figure 5: Plots of simulated $I(t)$ process in the first 25 days, Runs 1-6; $\lambda = 0.3, \mu = 0.1, \nu = 0.2$.

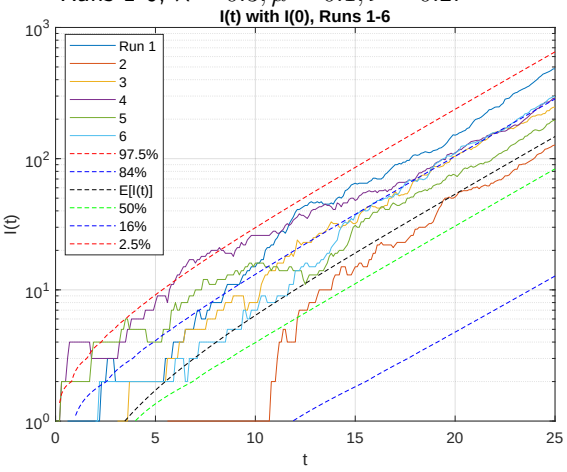

Figure 6: Semi-log plots of the $I(t)$ process, Runs 1-6; $\lambda = 0.3, \mu = 0.1, \nu = 0.2$.

normal (or Gaussian distribution); Thus, 68 percent and 95 percent confidence levels could be well approximated by the $\lambda \pm \sqrt{\lambda}$, and the $\lambda \pm 2\sqrt{\lambda}$, respectively.

The coefficient of variation of the Poisson process is given by

$$c_{A(t)} = \frac{1}{\sqrt{\nu t}}, \tag{25}$$

which converges to zero as $t \to \infty$. Thus, the arrival process $A(t)$ behaves much more predictably than the process $I(t)$, whose coefficient of variation remains on the order of unity at all t.

$$c_{I(t)} = \frac{1}{\sqrt{r\beta(t)}}, \tag{26}$$

where $r = \frac{\nu}{\lambda}$ and $\beta(t) \leq 1$ is defined in (12). As $t \to \infty$, $\beta(t) \to 1$, thus, the coefficient of deviation (CV) converges to $\frac{\lambda}{\mu}$, which, in our running example is $\sqrt{0.3/0.2} \approx 1.225$ as we discussed in Part I, p. 19, Example 3.

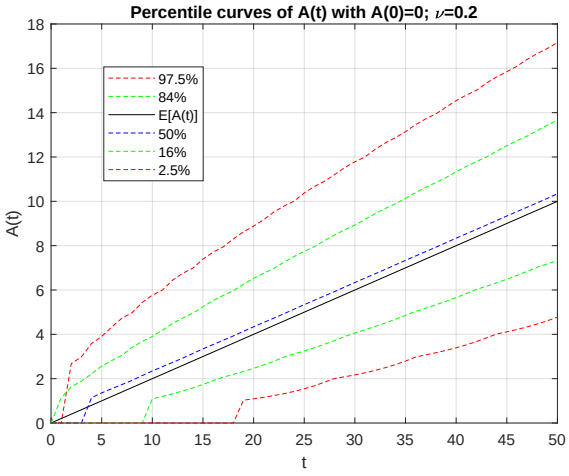

Figure 7: Percentile curves of Poisson process $A(t)$ of rate $\nu = 0.2$.

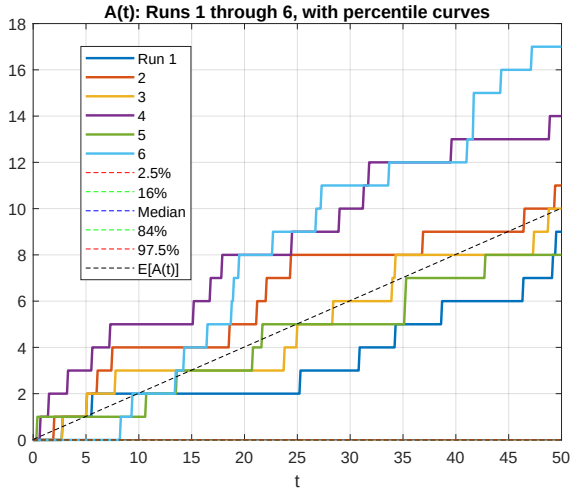

Figure 8: External arrival process $A(t)$, Runs 1-6.

2.3.3 Simulation of the processes $B(t)$ and $R(t)$

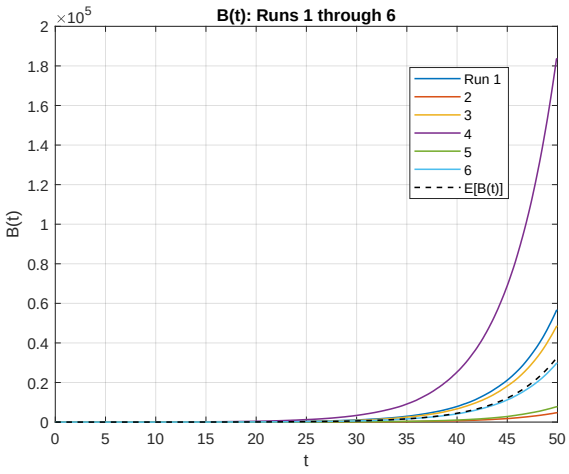

Figure 9: The process $B(t)$: Runs 1-6.

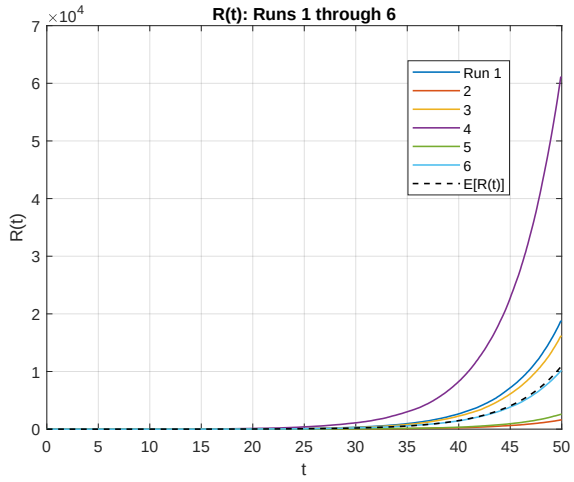

Figure 10: The process $R(t)$: Runs 1-6.

Although we were able to obtain the time-dependent probability mass function (PMF) of $I(t)$, it seems rather difficult to obtain closed form expressions of PMFs for the processes $B(t)$ and $R(t)$, although we can find their PGFs. It appears that we need to be content with approximate PMFs of $B(t)$ and $R(t)$. The technique we will explore is the saddle-point integration method, which Bernhard Riemann (1826-1866) pioneered in his pursuit of the famous 1859 conjecture, known as the Riemann Hypothesis [6]. We will report our full discussion of the processes $B(t)$ and $R(t)$ in Part IV [6].

In the present section we only show the results of the above six simulation runs, together with

[6] See, e.g., Harold M. Edwards, *Riemann's Zeta Function*, Dover Publications, Inc, 1974. Also `http://hp.hisashikobayashi.com/towards-a-proof-of-the-riemann-hypothesis-rh/` and references therein.

the stochastic means $\overline{B}(t)$ and $\overline{R}(t)$, which we obtained in Part I, viz:

$$\overline{B}(t) = \frac{\lambda}{a}(\overline{I}(t) - I_0 - \overline{A}(t), \tag{27}$$

$$\overline{R}(t) = \frac{\nu}{a}(\overline{I}(t) - I_0 - \overline{A}(t)), \tag{28}$$

As we can see, the process $B(t)$ and $R(t)$ also exhibit enormous variations across the runs. They are positively correlated with each other and with the $I(t)$ process, as well. Run 4 (magenta), Run 1 (blue) and Run 3 (yellow) are well above the mean curve, and Run 5 (green) and Run 2 (red) are below the mean in all the three processes $B(t), R(t)$ and $I(t)$. Run 6 (cyan) is just below the mean. The fact that these three processes behave in a similar fashion is quite expected, because both $\frac{dB(t)}{dt}$ and $\frac{dR(t)}{dt}$ are, on average, proportional[7] to $I(t)$ at a given time.

Referring to (2), $A(t)$ is much smaller than $I(t), B(t)$ and $R(t)$, except for the initial period, thus we have an approximate formula

$$I(t) \approx B(t) - R(t), \tag{30}$$

These large variations we observe in the processes $B(t)$, $R(t)$ and $I(t)$ are all consequences of the built-in *positive feedback loop* inherent to the internal infection process $B(t)$, which gives rise to exponential growth $\exp(at)$.

2.4 Other Important Statistical Data

In this section we discuss two additional topics for the benefits of the readers. One is how to derive the number of new infections for each day; the second is how to estimate the number of deaths.

2.4.1 Number of New Infections on Each Day

We take "day" as the time unit, as we do in our running examples throughout this report. We choose to interpret the interval $t \in (0, 1)$ as the 1st day, then the *number of newly infected persons* reported on the tth day, denoted as $N(t)$, should be computed as follows:

$$N(t) = B(t) - B(t-1) + A(t) - A(t-1), \tag{31}$$

By substituting the $\overline{B}(t)$ and $\overline{A}(t)$ obtained in Part I, we readily find the stochastic mean or the expected value of $N(t)$:

$$\overline{N}(t) \triangleq \mathsf{E}[N(t)] = \frac{\lambda\nu}{a^2}(1 - e^{-a})e^{at} - \frac{\lambda\nu}{a}. \tag{32}$$

For our running example of $a = \lambda - \mu = 0.3 - 0.1 = 0.2$, and $\nu = 0.2$, Figures 11 through 16 show the plots of the first 25 days and 50 days of three runs: Run-2, Run-4 and Run-6. These

[7] New internal infections (excluding the new arrivals from the outside), occur at the rate of $\lambda I(t)$, and recoveries/removals/deaths occur at the rate of $\mu I(t)$. Their expected values are related by the differential equations

$$\frac{d\overline{B}(t)}{dt} = \lambda\overline{I}(t) \quad \text{and} \quad \frac{d\overline{R}(t)}{dt} = \mu\overline{I}(t), \tag{29}$$

as shown in Part I, page 11 (27) and (31).

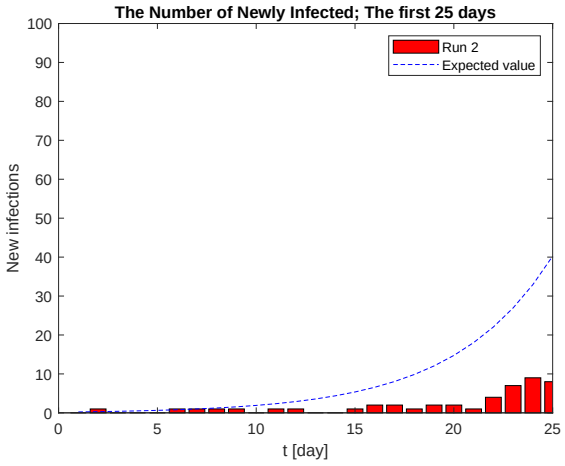

Figure 11: New infections on Daily-basis, Run-2, $\leq t \leq 25$.

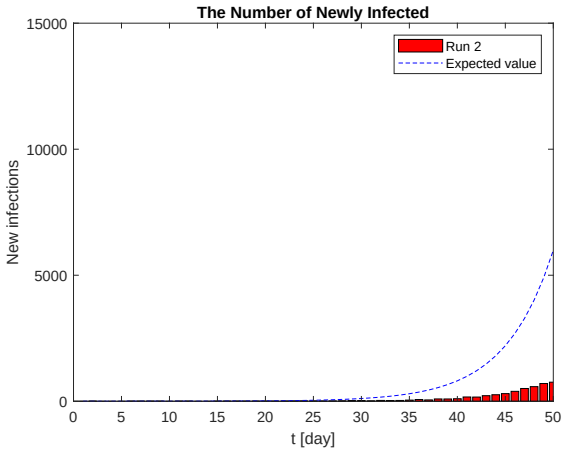

Figure 12: New infections on Daily-basis, Run-2, $\leq t \leq 50$.

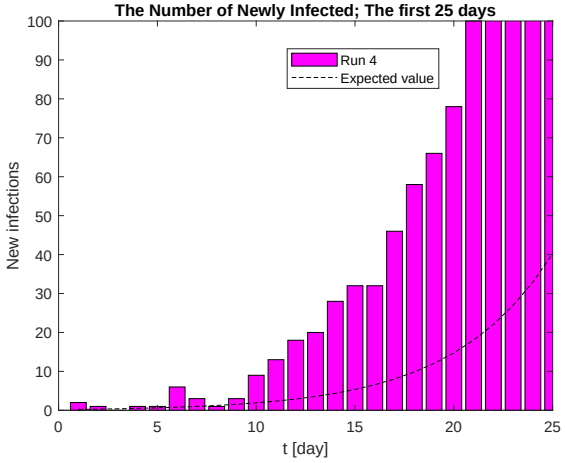

Figure 13: New infections on Daily-basis, Run-4, $\leq t \leq 25$.

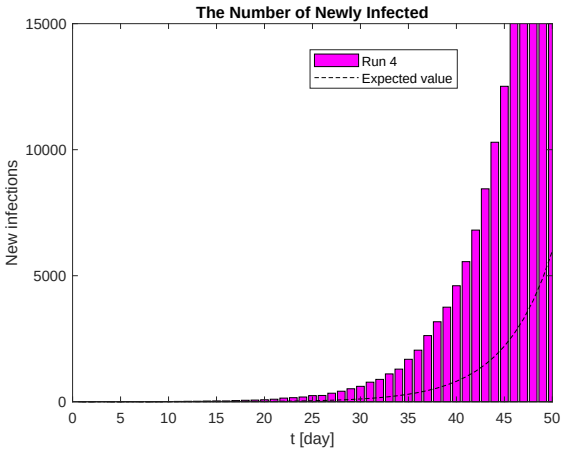

Figure 14: New infections on Daily-basis, Run-4, $\leq t \leq 50$.

simulations correspond to shown in the previous figures concerning the processes $I(t), B(t), R(t)$ and use the same colors as used in the curves. Run-2 (red) the highest; Run-4 (magenta) is the highest, exceeding the expected value $\mathsf{E}[N(t)]$ by factor of 4 or 5; Run-6 (blue) is close to the expectation. We observe enormous among among the 6 runs. In Appendix we show the remaining six runs. Since we have not yet obtained the PMFs for $B(t)$, we cannot compute the percentile curves at this point. But from these simulation runs, the variations among different runs seem even more pronounced than we observed in $I(t)$.

Note that for the short range $1 \leq t \leq 25$, the vertical axis range is [0, 100], whereas for $1 \leq \ t \leq 50$, the range is expanded by a factor of 150. This is consistent with the exponential growth of $\exp(at)$. From $t_1 = 25$ to $t_2 = 25$, it will grow by the factor of $\exp(a(t_2 - t_1)) = \exp(0.2 \times 25) = e^5 = 148.4$

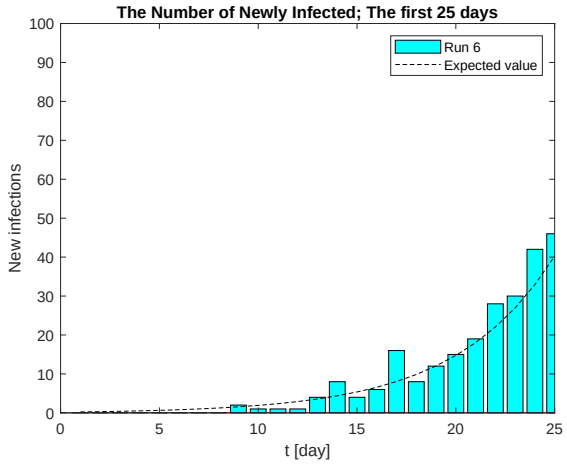

Figure 15: New infections on Daily-basis, Run-4, $\leq t \leq 25$.

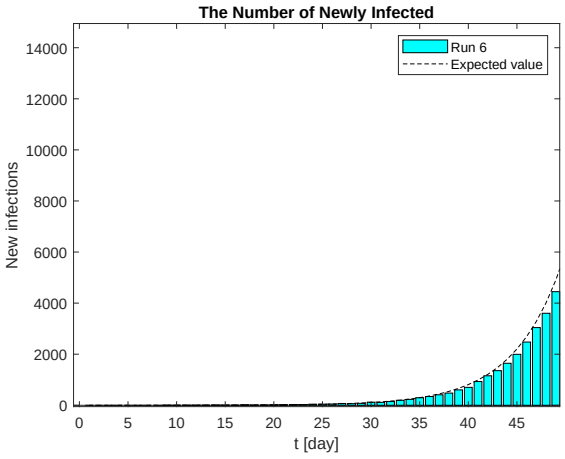

Figure 16: New infections on Daily-basis, Run-4, $\leq t \leq 50$.

2.4.2 Cumulative Number of Deaths

The most important aspect of any model of an infectious disease should be how to estimate or predict the number of deaths. In the current Covid-19 epidemic, the case fatality rate is reportedly less than one percent for young people but will be much higher for 60 years or older, and those with co-morbidity. In the present model, we assume a homogeneous population model, but the model can be generalized to multiple "classes" (or types), by assigning the model parameters ν_c, λ_c and μ_c for different classes of infected population. As an illustration, let us assume fr= 2% as an overall

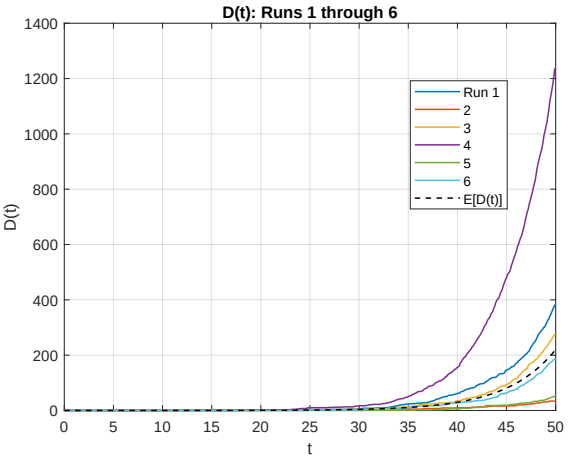

Figure 17: The cumulative of deaths $D(t)$: Runs 1-6, the fatality rate (fr) 2%.

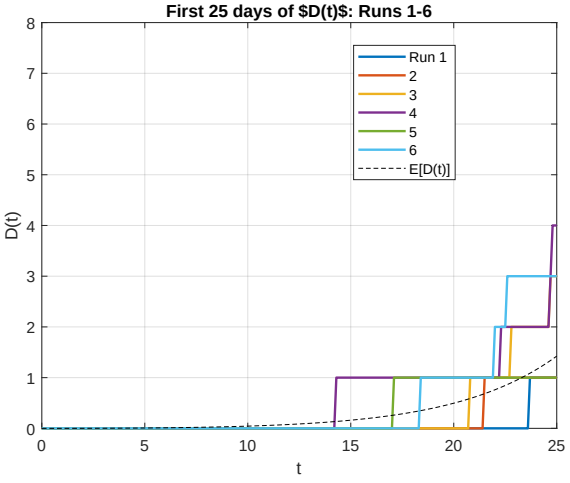

Figure 18: The first 25 days of $D(t)$: Runs 1-6.

fatality rate. Simulation of the death process $D(t)$ can be done by randomly splitting the process $R(t)$ with the specified fatality rate and produce $D(t)$ as a sub-process of $R(t)$. Figures 17 shows the result of the six runs. Figure 18 shows the first 25 days of the same $D(t)$.

3 The BDI Process $I(t)$ with the initial condition $I_0 \geq 1$

By looking at the semi-log plots of simulation runs of the process $I(t)$, some readers may wonder whether the huge variations among different runs may have to do with the fact that some simulation runs remain zero for a considerable period. This question can be answered by examining the process $I(t)$ with the initial condition $I_0 = 1$. In referring to (9), the second term represents the PGF of the BD process without immigration (ν=0), which is often referred to as the *simple birth-and-death process* or as *Feller-Arley (FA) process.* [8]

3.1 Analysis of the Modified Model

We rewrite (9) as

$$G_{BDI:I_0}(z,t) = G_{BDI:0}(z,t)G_{FA:I_0}(z,t), \tag{33}$$

where $G_{BDI:0}(z,t)$ is the PGF of the BDI process with the initial condition $I_0 = 0$, which we have studied thus far:

$$G_{BDI:0}(z,t) = \left(\frac{a}{\lambda e^{at} - \mu - \lambda(e^{at}-1)z}\right)^r \tag{34}$$

and

$$G_{FA:I_0}(z,t) = \left(\frac{\mu(e^{at}-1) + (\lambda - \mu e^{at})z}{\lambda e^{at} - \mu - \lambda(e^{at}-1)z}\right)^{I_0}. \tag{35}$$

The product form expression (33) means that the BDI process with nonzero I_0 is the sum of the two independent processes, whose PGFs are given by (34) and (35):

$$I_v = I_{BDI:0}(t) + I_{FA:I_0}(t). \tag{36}$$

By defining $\alpha(t)$ (see [9][10]) by

$$\alpha(t) \triangleq \frac{\mu(e^{at}-1)}{\lambda e^{at} - \mu} = \frac{\mu}{\lambda}\beta(t), \tag{37}$$

where $\beta(t)$ was earlier defined by (12), we can rewrite (35) as

$$G_{FA:I_0}(z,t) = \left(\frac{\alpha(t) + [1 - \alpha(t) - \beta(t)]\ z}{1 - \beta(t)z}\right)^{I_0}. \tag{38}$$

By taking the natural logarithm, differentiating w.r.t. z, and setting $z = 1$, we find the expected value of this random process:

$$\overline{I}_{FA:I_0}(t) \triangleq \mathsf{E}[I_{FA}(t)] = I_0\frac{(1-\alpha(t))}{(1-\beta(t))} = I_0 e^{at}, \tag{39}$$

[8] In his seminal paper of 1939 [7], W. Feller (1906-1970) introduced this process for the study of population growth of some species. N. Arley [8] applied this model to cascade showers in cosmic ray theory.

Similarly, we find

$$\sigma^2_{FA:I_0}(t) \triangleq \mathrm{Var}[I_{FA:I_0}(t)] = I_0 \frac{(1-\alpha(t))(\alpha(t)+\beta(t))}{(1-\beta(t))^2} = I_0(\lambda+\mu)e^{at}\frac{(e^{at}-1)}{a}. \tag{40}$$

which leads to the following expression, for the *coefficient of variation* (CV) of the FA process, when $a > 0$:

$$c_{FA:I_0}(t) \geq \sqrt{\frac{aI_0}{\lambda+\mu}}, \quad \text{for all} \quad t. \tag{41}$$

For the case of our running example with $\lambda = 0.3$ and $\mu = 0.1$, the RHS of the above becomes $\sqrt{I_0/2}$. When $I_0 = 1$, and the CV $c_{FA:1}(t) \approx 0.707$ for all t, which is comparable to the CV of the BDI process with $I_0 = 0$, which is $c_{BDI:0}(t) \approx r^{-1/2} = 1.225$ (See Part I, p. 19 Example 2).

3.1.1 When $I_0 = 1$:

For the case $I_0 = 1$, it is easy to expand the PGF (35) in powers of z^n, obtaining

$$P_0^{FA:1}(t) = \alpha(t) \tag{42}$$

$$P_n^{FA:1}(t) = (1-\alpha(t))(1-\beta(t))\beta^{n-1}(t), \quad \text{for} \quad n \geq 1. \tag{43}$$

We further analyze the above result depending (i) $a > 0$, (ii) $a < 0$, or (iii) $a = 0$.

(i) When $a = \lambda - \mu > 0$: We find

$$\lim_{t\to\infty} \alpha(t) = \frac{\mu}{\lambda} = R_0^{-1} < 1, \quad \text{and} \quad \lim_{t\to\infty} \beta(t) = 1, \tag{44}$$

where

$$R_0 = \frac{\lambda}{\mu} > 1 \tag{45}$$

is called the *basic reproduction number* in epidemiology, as defined in (32) of Part I. The distribution form of (43) is very similar to (16): it is a geometric distribution of the form $\propto \beta^n(t)$, with $\beta(t) \approx 1$, and has a long tail similar to Figures 7-12 in Part I.

(ii) When $a < 0$: We have

$$\lim_{t\to\infty} \alpha(t) = 1, \quad \text{and} \quad \lim_{t\to\infty} \beta(t) = \frac{\lambda}{\mu} = R_0 < 1, \tag{46}$$

(iii) When $a = 0$,(i.e., $\mu = \lambda$): We rearrange (37) as

$$\alpha(t) = \frac{\mu(e^{at}-1)}{\lambda(e^{at}+a}, \quad \text{and} \quad \beta(t) = \frac{\lambda(e^{at}-1)}{\lambda(e^{at}-1)+a}. \tag{47}$$

Divide both the denominator and the nominator by a, and let $a \to 0$. Using the familiar formula $\lim_{a\to 0}(e^{at}-1)/a = t$, we find

$$\alpha(t) = \beta(t) = \frac{\lambda t}{1+\lambda t}, \quad t \geq 0. \tag{48}$$

Rearrange the PGF (35) in a similar fashion, and we find

$$G_{FA:I_0}(z,t) = \left(\frac{\lambda t + (1-\lambda t)z}{1+\lambda t - \lambda t z}\right)^{I_0}, \tag{49}$$

from which we obtain

$$\overline{I}_{FA:I_0}(t) \triangleq \mathsf{E}[I_{FA:I_0}(t)] = I_0, \tag{50}$$

$$\sigma^2_{FA:I_0}(t) \triangleq \mathrm{Var}[I_{FA:I_0}(t)] = 2I_0\lambda t, \tag{51}$$

which could have been directly obtained from (39) and (40). The PMFs of (42) and (43) will be further simplified, when $\mu = \lambda$:

$$P_0^{FA:1}(t) = \frac{\lambda t}{1+\lambda t} \tag{52}$$

$$P_n^{FA:1}(t) = \frac{(\lambda t)^{n-1}}{(1+\lambda t)^{n+1}}, \quad \text{for} \quad n \geq 1. \tag{53}$$

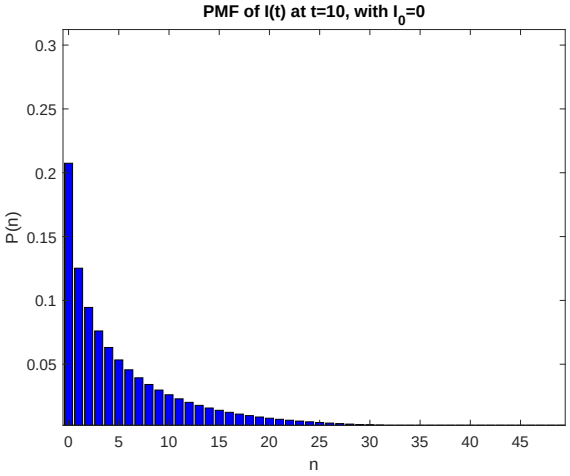

Figure 19: PMF of $I(t)$ at $t = 10$; $I_0 = 0$

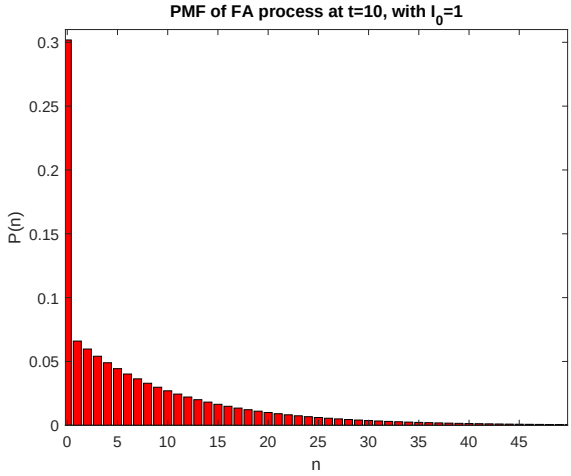

Figure 20: PMF of FA Process at $t = 10$, $I_0 = 1$

Referring to (16), the PMF of the BDI process with $I_0 = 1$ is given by the convolution of the two PMFs, for which we have found closed form expressions:

$$\begin{aligned} P_n^{BDI:1}(t) &= P_n^{BDI:0}(t) \otimes P_n^{FA:1}(t) \\ &= (1-\beta(t))^r \left[\sum_{k=0}^{n-1} \binom{k+r-1}{k}(1-\alpha(t))(1-\beta(t)\beta^{n-k-1}(t) + \binom{n+r-1}{n}\beta^n(t)\alpha(t)\right]. \end{aligned} \tag{54}$$

In Figure 19 is the PMF $P_n(t)$ of the $I(t)$ given in (16) at $t = 10$ for our running example, i.e. $a = 0.2$ and $r = 0.667$ (see Part I, P. 18, Figure 9). Figure 20 is the PMF (42) and (43). Figure 22 is the PDF of $I(t)$ with the initial condition $I_0 = 1$ given by (16). We computed this by computing

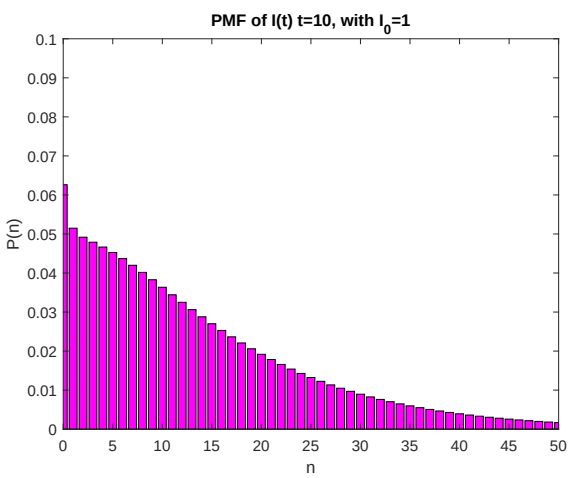

Figure 21: PMF of $I(t)$ at $t = 10$; $I_0 - 0$

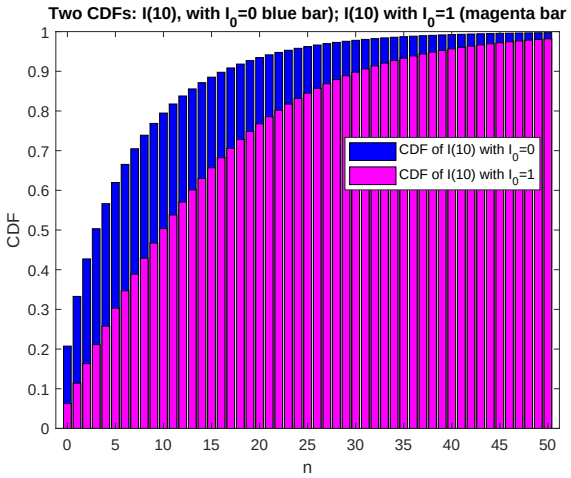

Figure 22: CDFs of $I(t)$ at $t = 10$,$I_0 = 0$ (in blue) $I_0 = 1$ (in Magenta)

the *convolution* of the above two PDFs, i.e., (54). Figure 22 shows the CDFs of $I(t)$ at $t = 0$, with $I_0 = 0$ (in blue) and with $I_0 = 1$ (in magenta).

For the CDF $F_X(x)$ of a non-negative random variable X, you can show the following simple formula: [9]

$$\int_0^\infty (1 - F_X(x))dx = \mathsf{E}[X], \tag{55}$$

Thus, the white area should be equal to $\overline{I}(t) = \frac{\nu}{a}(e^{at} - 1) = e^2 - 1 = 7.39 - 1 = 6.39$ at $t = 10$. Thus, the blue bar area behind the magenta bars should be equal to $I_0 e^{at} = e^2 = 7.39$, an increase in $\mathsf{E}[I(t)]$ at $t = 10$ due to the presence of an infected person at $t = 0$.

3.1.2 An efficient computation of the PMF of $I(t)$ with $I_0 = 1$

An alternative and computationally more efficient way to compute the $P_n^{BDI:1}$ will be presented below. We use alternative representation of the PGF (35) as follow

$$G_{FA:I_0}(z,t) = \left(\frac{1-\beta(t)}{1-\beta(t)z}\right)^{I_0} (1 - p(t) + p(t)z)^{I_0}, \tag{56}$$

where

$$p(t) = \frac{1-\alpha(t)-\beta(t)}{1-\alpha(t)} = \frac{\lambda - \mu e^{at}}{a}. \tag{57}$$

Then we can have an alternative product representation to (33), as follows.

$$G_{BDI:I_0}(z,t) = \left(\frac{1-\beta(t)}{1-\beta(t)z}\right)^{I_o+r} (1 - p(t) + p(t)z)^{I_0}. \tag{58}$$

[9] See e.g. , [5], pp. 73-74.

We may term the second term in the above product representation as the PGF of a *generalized binomial distribution* in the sense that the coefficients of z^n terms are not necessarily non-negative. For $I_0 = 1$, this term is extremely simple, having only two terms: $P_0(t) = 1 - p(t)$ and $P_1(t) = p(t)$, which makes the convolution extremely simple: Fig 23 and Figure 24 show the PDFs of the above two PGFs. Their convolution results in the PMF as shown in Figure 21.

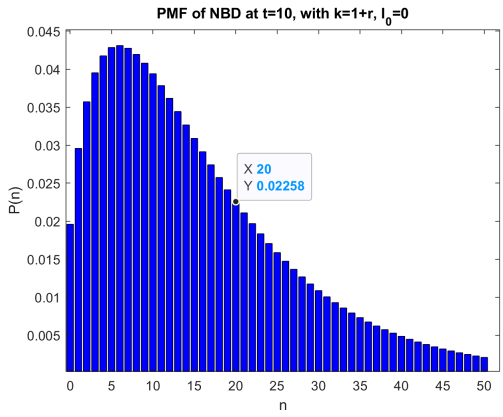

Figure 23: NBD with $k = 1 + r$

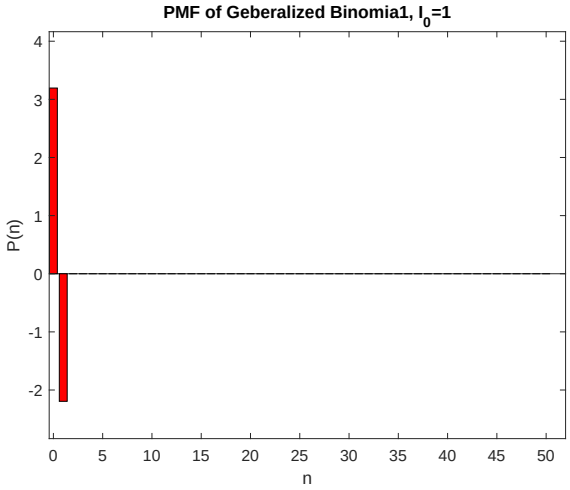

Figure 24: Generalized binomial distribution

3.2 Simulation Results

The percentile curves for the PMF $P_n(t)$ of $I(t)$ with the initial condition $I(0) = 1$ are plotted together with the mean $\overline{I}(t) \triangleq \mathsf{E}[I(t)]$ are shown in Figure 25 and its semi-log plots are given in Figure 26.

In Figure 27 we show six simulation runs with the initial condition $I(0) = 1$ and their semi-log plots in Figure 28. The large variances among the sample paths still persist, thus we do not see any fundamental differences from the case where the simulations start with the initial condition $I(0) = 0$. This conclusion is not unexpected, if we go back to Equation (36):

$$I_{BDI:I_0}(t) = I_{BDI:0}(t) + I_{FA:I_0}(t)., \tag{59}$$

in which we set $I_0 = 1$. Since the two processes are statistically independent, the sum of their variances is the variance of the summed process:

$$\sigma^2_{BDI:1}(t) = \sigma^2_{BDI:0}(t) + \sigma^2_{FA:1}(t), \tag{60}$$

where the first term on RHS is from Part I (53)

$$\sigma^2_{BDI:0}(t) = \frac{\nu(\lambda e^{at} - \mu)(e^{at} - 1)}{a^2} \approx \frac{\nu\lambda}{a^2} e^{2at}, \tag{61}$$

and the second term is from (40)

$$\sigma^2_{FA:1}(t) = (\lambda + \mu)e^{at}\frac{(e^{at} - 1)}{a} \approx \frac{(\lambda + \mu)}{a} e^{2at}, \tag{62}$$

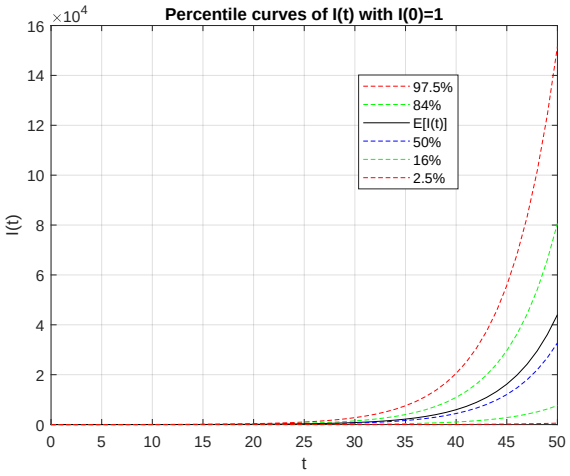

Figure 25: Percentile curves of $P_n(t)$ of $I(t)$ with $I(0) = 1$; $\lambda = 0.3, \mu = 0.1, \nu = 0.2$.

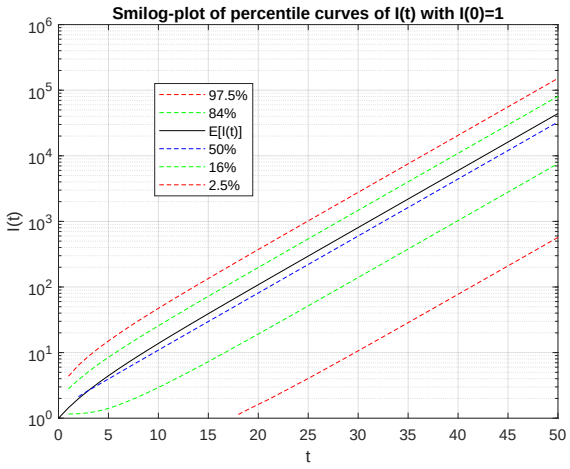

Figure 26: Semi-log plot of the percentile curves for $I(t)$ with $I(0) = 1$

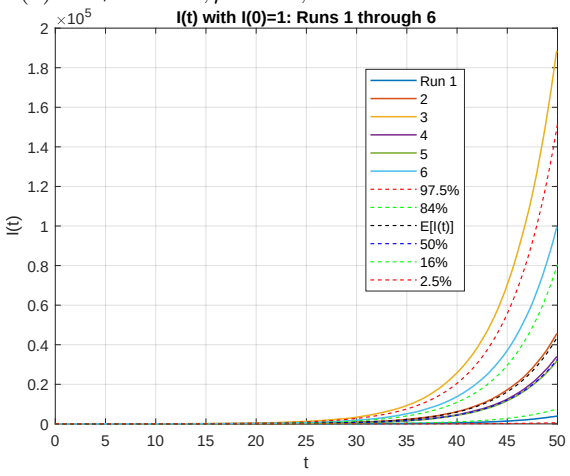

Figure 27: The $I(t)$ process with $I(0) = 1$, Runs 1-6; $\lambda = 0.3, \mu = 0.1, \nu = 0.2$.

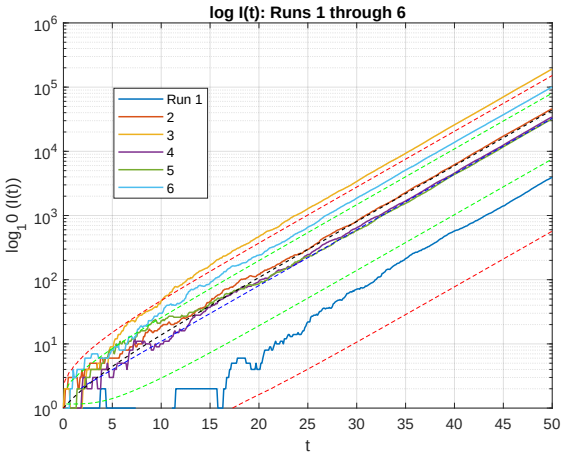

Figure 28: Semi-log plots of $I(t)$ with $I(0) = 1$, Runs 1-6; $\lambda = 0.3, \mu = 0.1, \nu = 0.2$.

which leads to

$$\sigma^2_{BDI:1}(t) \approx \left(\frac{\nu\lambda}{a^2} + \frac{(\lambda+\mu)}{a}\right) e^{2at} = \frac{(\nu+\lambda)\lambda - \mu^2}{(\lambda-\mu)^2} e^{2at}. \tag{63}$$

The expected value of the process $I(t)$ with $I(0) = 1$ is from (39)

$$\mathsf{E}[I_{BDI:1}(t)] = (1 + \frac{\nu}{a})e^{at} - \frac{\nu}{a} \approx \frac{\nu + \lambda - \mu}{\lambda - \mu} e^{at}, \tag{64}$$

Thus, the CV of the the process $I(t)$ remains constant for all t whether not the initial condition is zero or nonzero

$$c_{BDI:1}(t) = \frac{\sqrt{(nu+\lambda)\lambda - \mu^2}}{\lambda - \mu} = 1.87, \tag{65}$$

which is even larger than the CV of $I(t)$ with $I(0) = 0$, which is 1.225.

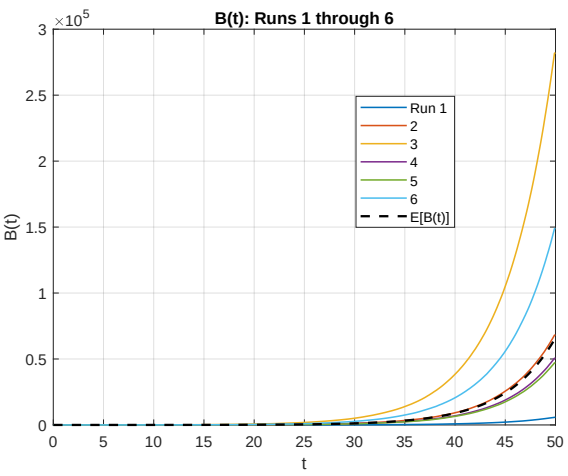

Figure 29: The process $B(t)$ with $I(0) = 1$: Runs 1-6.

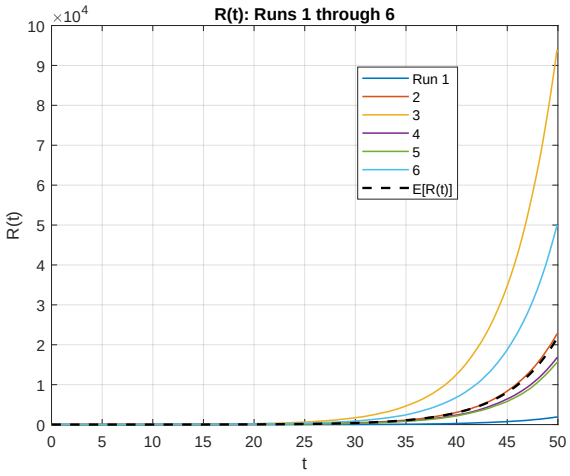

Figure 30: The process $R(t)$: Runs 1-6.

4 Concluding Remarks and Future Plans

In the present report, we have presented extensive simulation results by implementing a simulator in MATLAB of our stochastic model of an epidemic disease proposed in Part I [1]. The simulated infection process $I(t)$ indeed exhibits huge variations among many simulation runs.

In the current pandemic of COVID-19, most experts and policy makers seemingly are looking for all factors that might help them understand why they see such enormous disparities across their countries or in the world in terms of the magnitude of infected populations and death tolls. Our analysis and simulation shows that the epidemic process which has inherent positive feedback can have enormous variations, sometimes by factor of 100 or more, under an identical condition.

In both analysis and simulations we have so far assumed a homogeneous model, whether the model parameters (λ, μ and ν are constant. In Part III [11], we will report on our analysis of non-homogeneous (time varying) models, whereby we allow the model parameters $\lambda(t)$ and $\mu(t)$ to be arbitrary functions of time. This generalization will help us better understand, for instance, how a change in *social distancing* and/or an improvement or degradation in medical treatment will affect the infection process.

Part IV [6] will be devoted to use of saddle-point integration technique to approximately characterize the internal infection process $B(t)$ and the recovery process $R(t)$, which seem to defy an exact solution unlike the process $I(t)$ for which we have an exact time-dependent probability distribution function.

In Part V [2], we plan to develop a statistical theory to estimate the model parameters from real data of Covid-19 epidemics and demonstrate how our stochastic model can be used in predicting the stochastic behavior of an infectious disease. An application of the EM (expectation-maximization) algorithm to obtain maximum likelihood estimate from incomplete data will be explored.

Our BDI (birth-and-death-with-immigration) process based model should be extensible to more complex situations where we consider different types or classes of populations, in which class-c people will have different infectious rates and recovery rates, having λ_c, μ_c, although an exact analytic solution may be hard to come by, but a simulation model based on the BDI process should be rather straightforward, and we plan to pursue this important model. This type of generalization

is possible mainly because our model is linear unlike SIR and other models which seem dominant in mathematical epidemiology.

Acknowledgments

I thank Prof. Brian L. Mark of George Mason University for his valuable suggestions and help in the MATLAB simulation. Were it not for his kind help, I could not have completed this rather laborious study.

References

[1] H. Kobayashi, "Stochastic Modeling of an Infectious Disease: Part I: Understand the Negative Binomial Distriution and Predict an Epidemic More Reliably." `https://arxiv.org/pdf/2006.01586.pdf`, May 28 2020.

[2] H. Kobayashi, "Stochastic Modeling of an Infectious Disease: Part V: Maximum likelihood estimate of model parameters from real data, and validation of our model." `http://hp.hisashikobayashi.com`, (in preparation) 2020.

[3] H. Kobayashi, *Modeling and Analysis: An Introduction to System Performance Evaluation Methodology*. Addison Wesley, 1978.

[4] H. Kobayashi and B. L. Mark, *System Modeling and Analysis: Foundations for System Performance Evaluation*. Prentice Hall, 2008.

[5] H. Kobayashi, B. L. Mark and W. Turin, *Probability, Random Processes, and Statistical Analysis*. Cambridge University Press, 2012.

[6] H. Kobayashi, "Stochastic Modeling of an Infectious Disease: Part IV: Appeoximate nalysis of the Internal infection process $B(t)$ and other processes, based on saddle-point integration." `http://hp.hisashikobayashi.com`, (in preparation) 2020.

[7] W. Feller, "Die Grundlagen der Volterraschen Theorie des Kampfes ums Dasein in wahrscheinlichkeitstheoritischer Behandlung," *Acta Biotheoretica*, vol. 5, pp. 11–40, 1939.

[8] N. Arley, *On the theory of stochastic processes and their application to the theory of cosmic radiation*. Wiley, 1943.

[9] N. T. Bailey, *The Elements of Stochastic Processes With Applications to the Natural Sciences*. John Wiley & Sons, Inc., 1964.

[10] H. Takagi, "Lecture Note: Bith-and-Death Process and Its Application (in Japanese)," March 2007.

[11] H. Kobayashi, "Stochastic Modeling of an Infectious Disease: Part III: Non-homogenous (or time-varying) models and control of the infection process." `http://hp.hisashikobayashi.com`, (in preparation) 2020.

